IEEE Journal of Microwaves

Received 5 November 2021; accepted 16 November 2021. Date of publication 24 December 2021; date of current version 7 January 2022.

*Digital Object Identifier 10.1109/JMW.2021.3130765*

# Terrestrial Microwave Power Beaming

**CHRISTOPHER T. RODENBECK [1] (Fellow, IEEE), BRIAN B. TIERNEY [1] (Member, IEEE), JAMES PARK [1], MARK G. PARENT [1], CHRISTOPHER B. DEPUMA [1], CHANDLER J. BAUDER [1] (Graduate Student Member, IEEE), THOMAS J. PIZZILLO [1], PAUL I. JAFFE [1] (Senior Member, IEEE), BRIAN H. SIMAKAUSKAS [2], AND TREVOR MAYHAN [1]**

*(Regular Paper)*

[1]Naval Research Laboratory, Washington, DC 20375-5307 USA
[2]MIT Lincoln Laboratory, Lexington, MA 02421 USA

CORRESPONDING AUTHOR: Christopher T. Rodenbeck (e-mail: chris.rodenbeck@ieee.org).

This work was supported by the Office of the Undersecretary of Defense for Research and Engineering's Operational Energy Capability Improvement Fund.
This article has supplementary downloadable material available at https://ieeexplore.ieee.org/document/9662403/media#media, provided by the authors.

**ABSTRACT** This paper establishes the practicality of terrestrial microwave power beaming at distances >1 km. To beam microwave power along the surface of the earth, it is necessary to consider and, where possible, exploit the effects of microwave propagation across terrain. Key design considerations include the effect of scattering from surface topography, approaches for characterizing the beam in the presence of multipath, safety, and efficiency. A rapid demonstration at the US Army Research Field in Blossom Point, MD, delivers 1.6 kW of electrical power at a 1046 m standoff from a 5.4-m-diameter X band transmitter. The transmitter is a reflector antenna with a linearly actuated feed horn that can focus the power density at specific standoff distances. Experimental results over cluttered, irregular terrain achieve a 2.3 dB (70%) enhancement in power density at the target site by deliberate exploitation of a ground bounce. A 4 $m^2$ rectenna receiver produces the 1.6 kW of output power at a 73% RF-to-DC conversion efficiency, which exceeds the current state of the art at X band. In addition, a test to destruction of 4 large rectenna arrays demonstrates how overvoltage protection circuits can improve the RF power handling of rectenna arrays by >1 dB. A final experiment demonstrates >1 kW delivered at >1 km distance to a light display. Since these results should readily scale to higher levels of power and performance, recommendations are provided to mature the technology for operational use.

**INDEX TERMS** Wireless power transmission, microwave power transmission, power beaming, rectennas, rectenna arrays, radiofrequency safety.

## I. INTRODUCTION

*Microwave power beaming* is the efficient point-to-point transfer of electrical energy across free space by a directive microwave beam. A recent publication [1] provides an overview of the progress to-date in the field and motivating factors – including, prominently, the eventual use of microwave power beaming for space-to-earth wireless power transmission (WPT). This paper explores the application of microwave power beaming to energy transfer along the surface of the earth. Fig. 1 illustrates the concept: a ground-based microwave transmitter directed towards the horizon illuminates a rectenna (rectifying antenna) array that converts the incident microwave power to DC voltage. Since microwave scattering from the terrain is a major design consideration, this application is therefore classified as *terrestrial microwave*


**FIGURE 1.** A terrestrial microwave power beaming link.

*power beaming*. Recent articles across the media indicate rising interest in the topic [2]–[7].

Prior terrestrial demonstrations at distances > 500 m have minimized terrain scattering effects by significantly elevating the transmit aperture and rectenna array [1], [8], [9] and by positioning the beam's target across a chasm on a mountainside [8]. However, in many practical scenarios, it could be desirable to beam power across arbitrary terrain while minimizing structural costs.

This paper describes a rapid demonstration of microwave power beaming across irregular, inhomogeneous terrain. To the authors' knowledge, this is the first power beaming demonstration to exploit the effect of "ground bounce" to enhance power density at the target location, and the first demonstration exceeding 1 km in range and 1 kW in received power at a frequency >2.5 GHz. The paper is organized as follows: Section II describes the test site, the transmitter, and the rectenna array. Section III presents an approach for the design and characterization of power beaming links that takes into account the effect of surface scattering; safety is also considered. Section IV describes the experimental results and provides a comparison to prior results. Additionally, a test to destruction evaluates competing approaches for overvoltage protection at the rectenna load. Section V provides recommendations for further technology development. Section IV concludes this paper.

## II. TECHNICAL APPROACH

The demonstrations presented in this paper are the result of a 13-month effort to show the feasibility to wirelessly deliver >1 kW of electrical power at a distance >1 km across terrain. Due to limited access – during the COVID-19 pandemic – to a suitable kW-class continuous wave (CW) microwave source, these demonstrations are executed using pulsed sources at two different sites. The primary site at the US Army Research Field in Blossom Point, MD, USA provides realistic terrain and the opportunity to test with a practically sized transmit aperture. An additional test site at the MIT Haystack Observatory in Westford, MA, USA operates at a much higher duty factor, making it possible to visually demonstrate the power transfer using a LED display.

The following section describes both test sites and the associated rectenna technology.

### A. PRIMARY TEST SITE: BLOSSOM POINT, MD, USA

Fig. 2a illustrates the Blossom Point test site using topographical data downloaded from the US Geological Survey [10]. The elevation is referenced to the global mean sea level. The transmit and receive locations are separated by 1046 m. Fig. 2b illustrates the terrain profile along a line of sight from the transmitter to the receiver. The terrain along this contour is rugged and nonhomogeneous, consisting of moist grassland, rocky soil, a gravel roadbed, concrete pads, and abandoned metal detritus. The resolution of the data is 1/3 arcsec in latitude and longitude [11], with an accuracy, at 95% confidence in the presence of vegetation, of 58 mm in height [12].

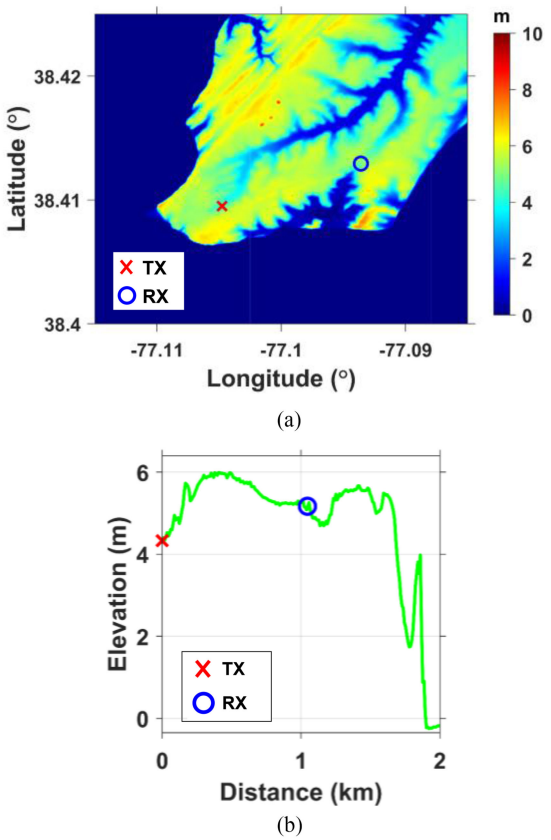


**FIGURE 2.** (a) Elevation above sea level at Blossom Point. The transmit (TX) and receive (RX) locations are separated by 1046 m. (b) Elevation above sea level along a line of sight between the TX and RX locations.

The transmit aperture shown in Fig. 3 is a 5.4-m-diameter parabolic reflector originally designed as a Cassegrain antenna but reconfigured to use a standard axial feed. The reflector's focal length is 2 m. The feed is a horn that illuminates the reflector with a 17 dB amplitude taper from the center to the edge. The horn is mounted on a linear actuator that allows the feed location to vary over a 100 mm range along the reflector's axis. Displacing the feed in this way creates a quadratic phase error across the reflector that can be used to focus the transmit beam at specific near field distances along the main beam axis [13]–[16]. As shown in this paper, the technique provides a capability to focus and finely adjust power density at a near-field target location, even in the presence of significant terrain scattering. The microwave source is a 9.7 GHz, 100 kW magnetron oscillator from Applied Systems Engineering, Inc. Under typical operating conditions, the maximum pulse duration is 1 $\mu$s at a 604 Hz repetition rate.

### B. RECTENNA ARRAY

The rectenna array is based on the individual rectenna element shown in Fig. 4a. The element consists of (*i*) a microstrip patch antenna fabricated using 18-$\mu$m-thick copper on a 0.51-mm Rogers 3003 substrate, (*ii*) a MACOM MA4E1317 Schottky diode, and (*iii*) microstrip features for impedance matching and harmonic tuning at 9.7-GHz as well as the 2$^{nd}$ and 3$^{rd}$

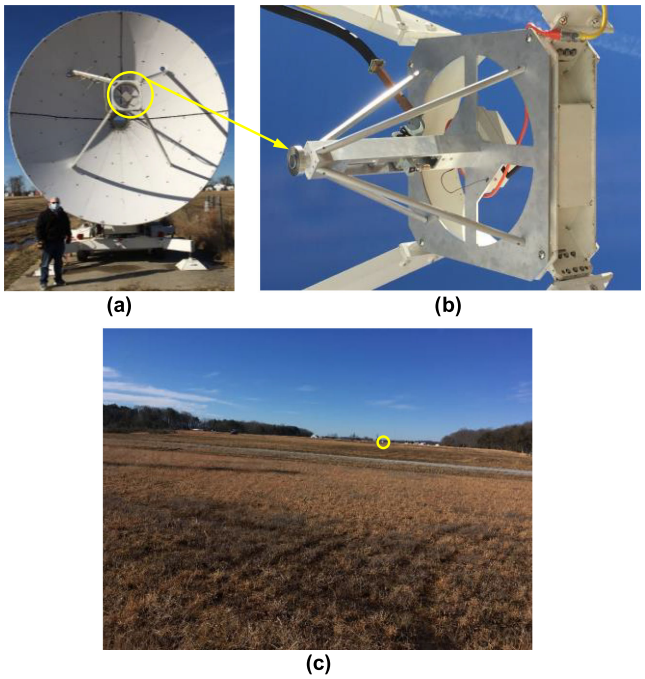


**FIGURE 3.** The transmit aperture is (a) a 5.4-m-diameter parabolic reflector fed by (b) a linearly actuated horn. Varying the feed location makes it possible to focus the beam at specific standoff distances from the transmitter. (c) A view of the transmitter from the target site 1046 m away.

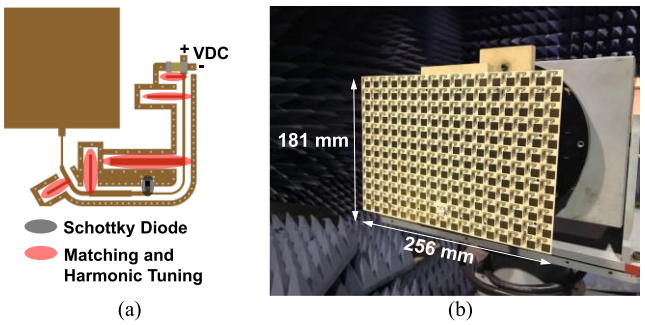


**FIGURE 4.** (a) The individual rectenna element, including the patch antenna, Schottky diode, and matching and harmonic tuning features. (b) The DC output of 203 rectenna elements combine to form a 181 mm x 256 mm rectenna tile. The DC connections take place on lower substrate layers.

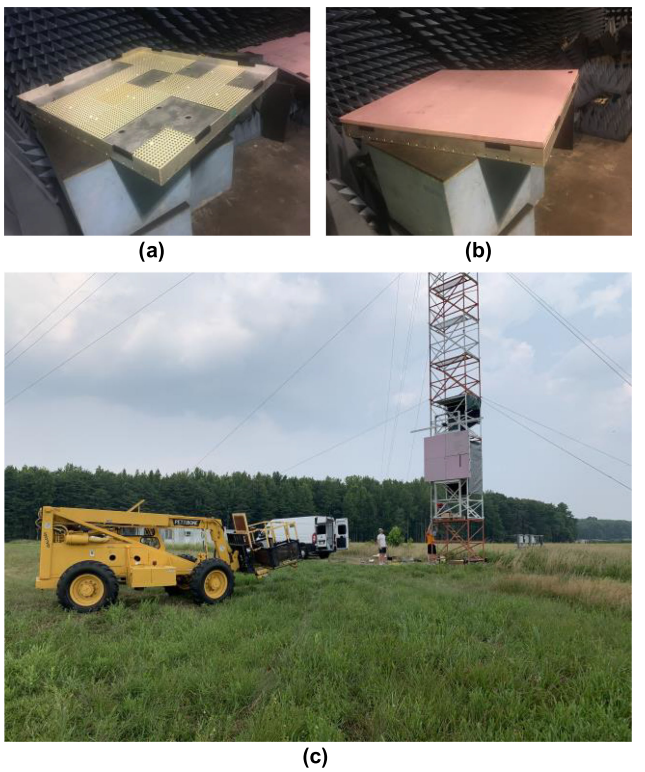


**FIGURE 5.** (a) 24 rectenna tiles being assembled into a quadrant. (b) The assembled quadrant with a protective radome installed. (c) Four quadrants installed at the Blossom Point target location.

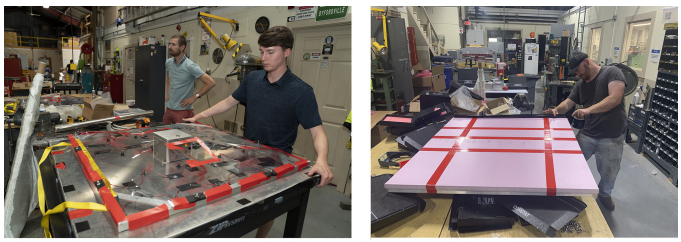


**FIGURE 6.** For the test at MIT, the rectennas are environmentally protected on the (a) rear and (b) front faces, allowing the arrays to withstand two severe thunderstorms between installation and the final test event.

harmonics. A 2-pF capacitor is also included to filter out any RF power not reflected by the harmonic stubs. Each tile has 12 rows of 17 rectenna elements whose DC outputs connect in parallel on a lower substrate layer; 12 of these rows connect in series to form the 181 mm × 256 mm, 203-element tileshown in Fig. 4b.

4 rows of 6 parallel-connected tiles combine in series to form a 1.02 m x 1.09 m rectenna quadrant. Fig. 5a illustrates a quadrant in the process of assembly. A radome fabricated using 25.4-mm-thick extruded polyurethane foam protects the assembled quadrant from unintentional damage during transport and installation, as shown in Fig. 5b. Four quadrants are connected in parallel and installed as shown in Fig. 5c at the target location at Blossom Point.

### *C. ADDITIONAL TEST SITE: MIT HUSIR*

The Haystack Ultrawideband Satellite Imaging Radar (HUSIR) transmitter [17] at the Massachusetts Institute of Technology (MIT) uses a 36.6 m circularly polarized Cassegrain antenna. The peak transmit power varies from 210 to 232 kW at 10.5 GHz when operated at a duty factor of 8.19%. This duty factor makes it possible to demonstrate the X-band rectenna technology at >1 km standoff, but with higher average power than is available at Blossom Point. A 2.06 m x 2.19 m circularly polarized variant of the Blossom Point rectenna is designed at a center frequency of 10.5-GHz for operation with HUSIR. As illustrated in Fig. 6, the front of each rectenna quadrant is protected by a polyurethane foam radome, as at Blossom Point, and the entire assembly is sealed

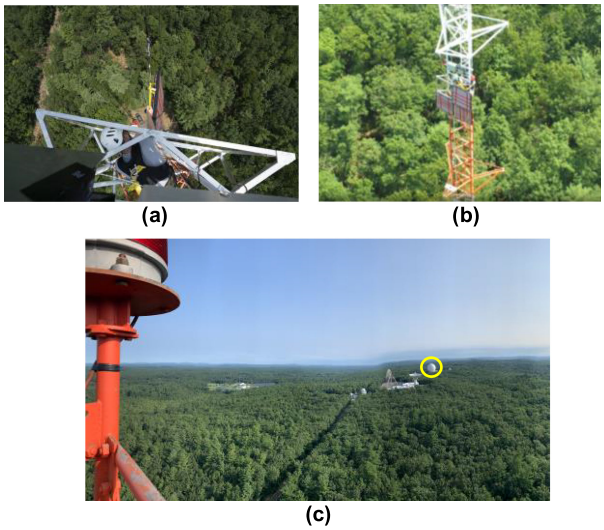


**FIGURE 7.** In (a) and (b), the rectenna array is installed 70.6 m above ground level 1141 m away from the HUSIR transmitter. (c) A view of HUSIR from the rectenna.

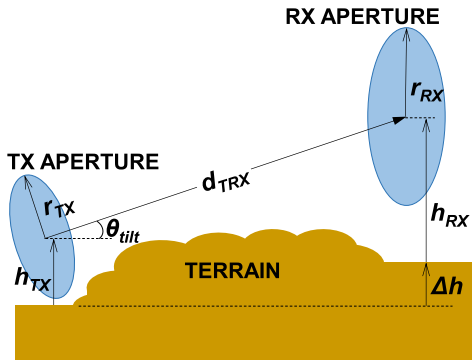


**FIGURE 8.** Design parameters for a power beaming link from a transmit (TX) aperture to a receive (RX) aperture across terrain.

with 1-mm-thick Mylar film, enabling the array to survive undamaged through 2 severe thunderstorms from the time of installation to the final test event.

As shown in Fig. 7, the rectenna array is installed 70.6 m above ground level at 1141 m away from the HUSIR transmitter. At this height, the center of the rectenna array is 30.4 m above HUSIR's phase center.

## III. PROPAGATION ANALYSIS

This section presents an approach (*i*) to optimize power beaming link geometry and (*ii*) to characterize the beam – taking into account the effect of scattering from the terrain. The transmit aperture and surface topography at the Blossom Point test site, described in the prior section, are used as a case study. Safety issues are also considered.

### A. TERRESTRIAL POWER BEAMING LINK DESIGN

Fig. 8 illustrates the geometry of a power beaming link across terrain. Relevant parameters include the transmit and receive aperture radii $r_{TX}$ and $r_{RX}$, the transmit and receive aperture

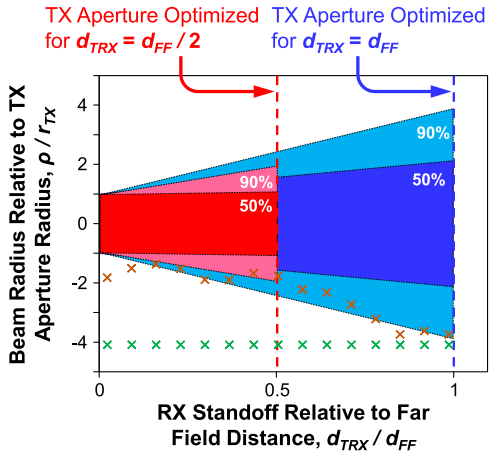


**FIGURE 9.** Approximate 50%-power and 90%-power cross sections for a beam emanating from a transmit aperture focused at the far field distance and at 1/2 the far field distance. Notional terrain profiles are plotted using "×" marks.

heights $h_{TX}$ and $h_{RX}$ above the local ground, the difference in ground elevation at the transmit and receive locations $\Delta h$, and the distance between the transmit and receive apertures $d_{TRX}$. Although both apertures could have a tilt in elevation angle $\theta_{tilt}$, only the transmit aperture tilts in this illustration.

A basic question for a terrestrial power beaming link is whether the effect of terrain scattering can be ignored, without the need to perform a detailed analysis. Unfortunately, design rules of thumb such as Fresnel zones [18] and popular approximations for mobile communications [19], [20], can be highly inaccurate for power beaming scenarios, producing overly conservative guidance for selecting antenna heights. As an alternative, the transmit beam can be approximated as a conic section extending from the transmit aperture to the target location. For a transmit aperture having an amplitude and phase distribution optimized to focus power at a distance $d_{TRX}$, the Gaussian beam approximation in [1] can be used to estimate the beam radius $\rho$ at $d_{TRX}$:

$$\rho = \frac{8}{\pi}\frac{d_{TRX}}{d_{FF}} r_{TX} \sqrt{\ln\left(\frac{1}{1-\eta}\right)} \tag{1}$$

where $d_{FF}$ is the transmit aperture's far field distance [20] and $\eta$ is proportion of the transmit power contained within $\rho$.

Fig. 9 illustrates two cases in which the transmit aperture is optimized to focus power at the far field distance and half the far field distance, respectively. In both cases, conic sections approximating the beam are shown for 50% and 90% of the beam power. Note that the 50% and 90% beam radii can alternatively be estimated using the expected Fresnel-region 3-dB and 10-dB beam widths, respectively, if the transmit aperture distribution deviates significantly from the ideal distribution [1] used to calculate (1). Selected peaks of the surface topology can be plotted on this chart, with appropriate rotation if $\theta_{tilt} \neq 0°$. The figure clearly illustrates that, even for power beaming over a flat surface, it can be necessary to significantly elevate the transmitter (or to up-tilt the transmitter and elevate

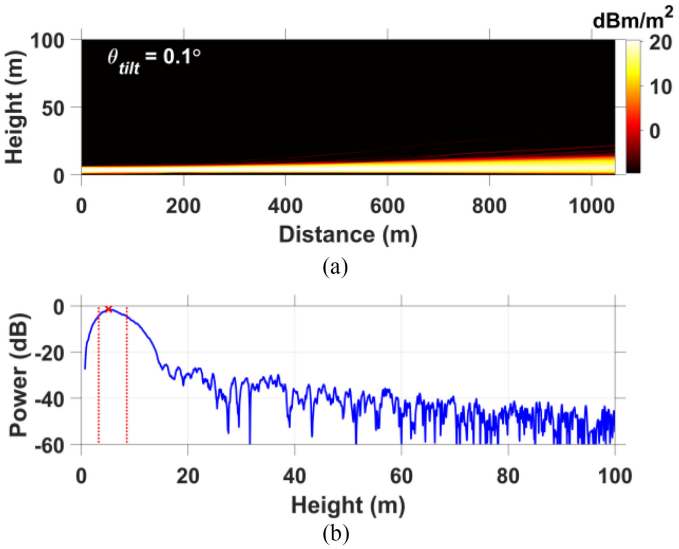


**FIGURE 10.** Screenshot from a movie (available online at https://ieeexplore.ieee.org/document/9662403/media#media) illustrating the variation in power density vs. height above ground as the transmitter tilt angle $\theta_{tilt}$ scans over a ±1° range: (a) Beam cross section for a transmit power of 1 W. As the beam passes through the ±0.1° range, the ground scattering enhances power density at the target location. (b) Power density vs height at $d_{TRX}$ = 1046 m normalized to the angle of maximum response, with peak and 3-dB points indicated.

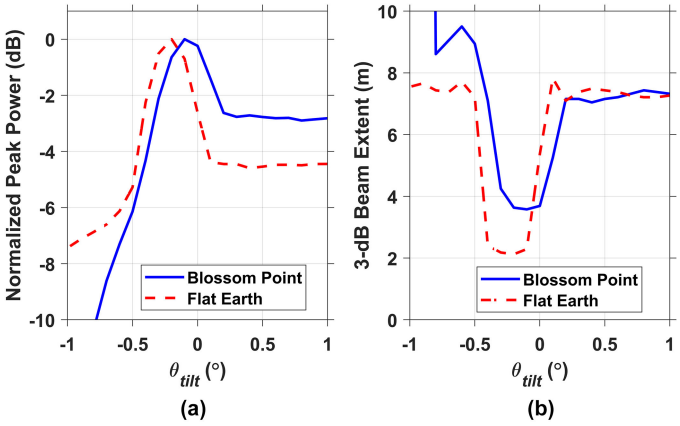


**FIGURE 11.** (a) Peak power and (b) 3-dB beam extent vs. tilt angle at $d_{TRX}$ = 1046 m. Results over a flat earth are provided for comparison.

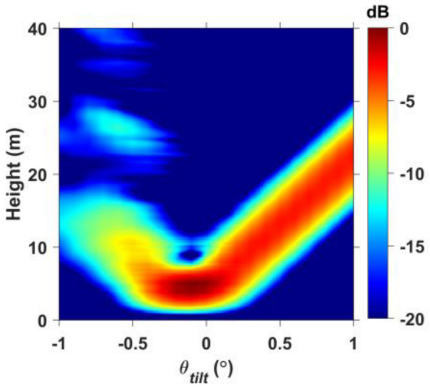


**FIGURE 12.** Plotting the power density at $d_{TRX}$ = 1046 m vs. height ($h_{RX}$ + $\Delta h$) and vs. $\theta_{tilt}$ shows that the optimum receiver height is 5 m over a −0.2° to +0.1° range of transmitter tilt angles $\theta_{tilt}$. The result is normalized to the peak response.

the receiver) to prevent terrain from intruding into the 90% beam cross section. For long range links, the structural costs could be significant.

Instead of constraining the geometry to minimize terrain scattering, it is possible to design a power beaming link to exploit scattering from terrain in order to achieve higher power density at the target location. The parabolic wave equation [21], [22] is a numerical method that can be used to explore propagation effects across terrain. Since this technique uses a paraxial approximation to the Helmholtz equation, it is valid in the Fresnel region and therefore well-suited for power beaming applications. For the Blossom Point transmitter described in Section II, $r_{TX} = 2.7$ m, $h_{TX} = 3.71$ m, $d_{TRX} = 1046$ m, $\Delta h = 0.8$ m, and $r_{TX}$ should be sized based on the predicted beam spotlight at $d_{TRX}$. Fig. 2 specifies the terrain, and $h_{RX}$ and $\theta_{tilt}$ are the design parameters. The movie shown in Fig. 10a powerfully illustrates the variation in power density vs. height at $d_{TRX} = 1046$ m as $\theta_{tilt}$ scans from $+1°$ to $-1°$. The height above ground is referenced to a zero at the location of the transmitter, and the soil is assumed to be uniform and dry with 0.67 S/m conductivity and a relative dielectric constant of 25.916. As the beam passes through the $\pm 0.1°$ range, the ground scattering actually improves the beam focus at the target location. Note that the approximations in this analysis include a reduction of the terrain model to a homogeneous 2-D cross section.

Fig. 11 calculates the peak power and 3-dB beam extent over the $\theta_{tilt} = \pm 1°$ range for the Blossom Point terrain, predicting a 2.73 dB increase in maximum power density for $\theta_{tilt} = -0.2°$ to $+0.1°$. The results over perfectly flat terrain, provided for comparison, show a > 4dB improvement is possible. Modifying the simulation so that flat earth is perfectly conducting increases the "ground bounce" effect to 5.75 dB, which approaches the theoretical limit of 6 dB [23].

Fig. 12 plots the power density as a function of height relative to the transmitter ground level ($h_{RX} + \Delta h$) and $\theta_{tilt}$ to graphically represent the optimum link geometry. For the Blossom Point link, a receiver height of 5 m is optimal over a $\theta_{tilt} = -0.2°$ to $+0.1°$ range of transmitter tilt angles. Referencing these parameters to the diagram in Fig. 11, $\theta_{tilt} = +0.1°$ provides a direct line of site to $h_{RX} = 5$ m, indicating that the optimum geometry uses this height with a slight downward tilt from the line of sight. This result is not general, however. Although not shown here, the optimal choice of receiver height and transmitter tile can be sensitive to small variations in link distance $d_{TRX}$. The analysis in Figs. 11 and 12 must be repeated or parameterized vs. $d_{TRX}$ if standoff distance is a design variable.

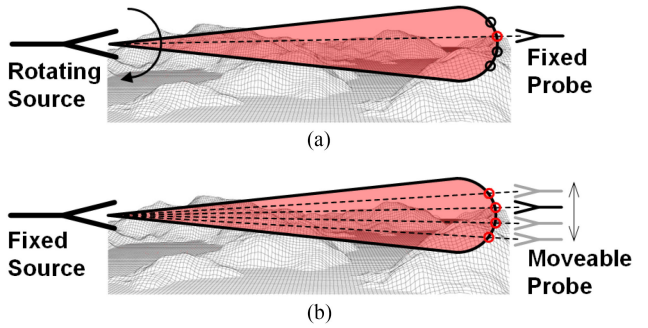


**FIGURE 13.** Characterizing the transmit beam using (a) a rotating source and fixed probe antenna and (b) using a fixed source and a probe antenna able to translate within the plane of the receive aperture. The measurements are not equivalent since the method in (a) samples the multipath along a single line of sight.

### B. BEAM CHARACTERIZATION

Terrain scattering impacts the measurement strategy for characterizing power density, and therefore efficiency, of a power beaming link. Fig. 13 illustrates two possible approaches. In Fig. 13a, a stationary field probe samples received power as the microwave source rotates in angle. In Fig. 13b, the microwave source remains fixed while the field probe translates linearly to sample power in the receive plane. In free space or in an anechoic chamber, the two techniques yield equivalent results. In the presence of terrain scattering, however, the approach in Fig. 13a samples all the points of the radiation pattern along the same line of sight and thus cannot capture the true variation in terrain scattering across the receive aperture. Even for highly directive transmit sources, scattering from terrain can be significant, making it necessary to spatially sample the beam, as shown in Fig. 13b, to accurately determine the incident power. The approach in Fig. 13a nonetheless does have physical meaning, from the standpoint of beam alignment, as the representation of the variation in rectenna output power as the transmitter scans its beam in angular space.

Both measurement approaches can be executed using the experimental setup shown in Fig. 14, which allows a horn antenna to translate to any position in the plane of the receive aperture over a $\pm 1.5$ m range in the horizontal dimension and over a 4 to 7 m range above ground in the vertical dimension.

### C. SAFETY

Time-averaged RF power density levels at 10 GHz are restricted by international agreement [24]–[26] to 10 W/m$^2$ for the general public, 50 W/m$^2$ for occupational exposure, and 100 W/m$^2$ for military workplaces. Due to its low duty factor, the Blossom Point transmitter's time-average radiated power only reaches these levels of concern in the immediate vicinity of the reflector's feed. For illustration, however, Fig. 15 maps these safety limits in the elevation plane assuming continuous transmit power. For this simulation, the transmitter tilt angle is 0.1°, and the results are scaled based on measured observations of the pulsed waveform at a distance of 1046 m. Referring to the figure, the boundary of the 100 W/m$^2$ exposure zone is within 3 m altitude (relative to the elevation at the transmitter) for distances within 3.7 km of the source. For practical applications, adequately sizing the rectenna to block this field at ground level would thus be important for minimizing RF exposure concerns further down range. Fig. 15 also shows significant field strength at altitudes $> 40$ m – where safety concerns are typically addressed by estimated duration of aircraft exposure during flight, as for the HUSIR system [27].

**FIGURE 14.** Experimental setup for characterizing power density in the plane of the receive aperture. A horn antenna probe translates horizontally over a $\pm 1.5$ m range and vertically over a 4 to 7 m range above ground level.

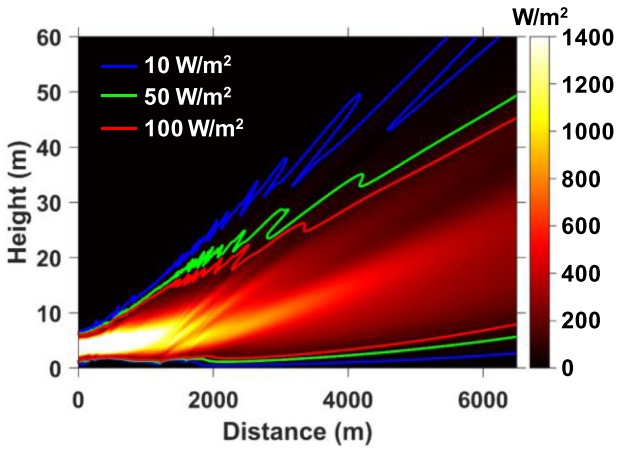


**FIGURE 15.** Plot of the 10, 50 and 100 W/m$^2$ exposure limit zones for the Blossom Point transmitter overlaid on a simulation of the power density in the elevation plane – assuming a continuous 100 kW source and no rectenna blockage.

## IV. EXPERIMENTAL RESULTS

The experimental results provided in this section demonstrate: (*i*) the usefulness of terrain effects for enhancing transmit power density at the receiver, (ii) $>1.6$ kW of electrical power

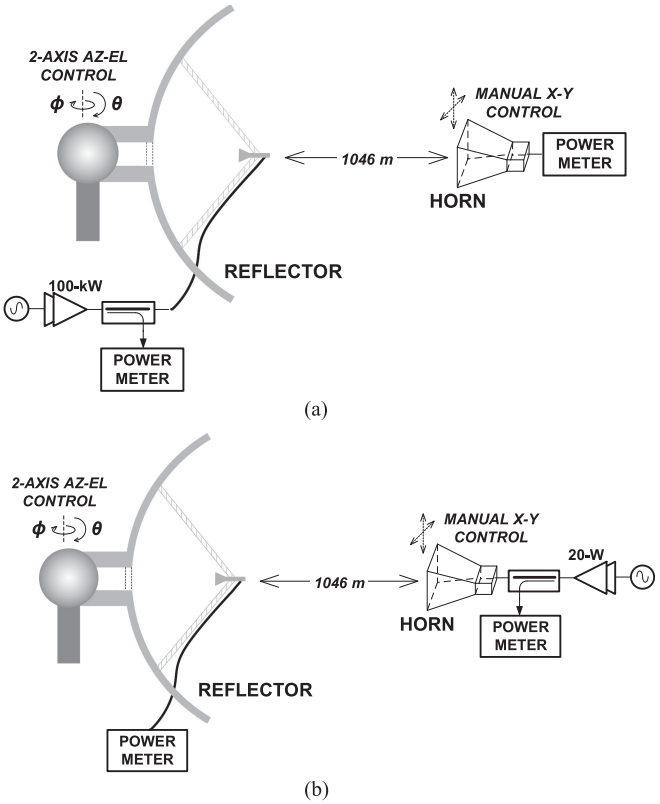


**FIGURE 16.** Experimental setups for characterizing the power beaming link where the reflector configured (a) as a transmitter and (b) as a receiver.

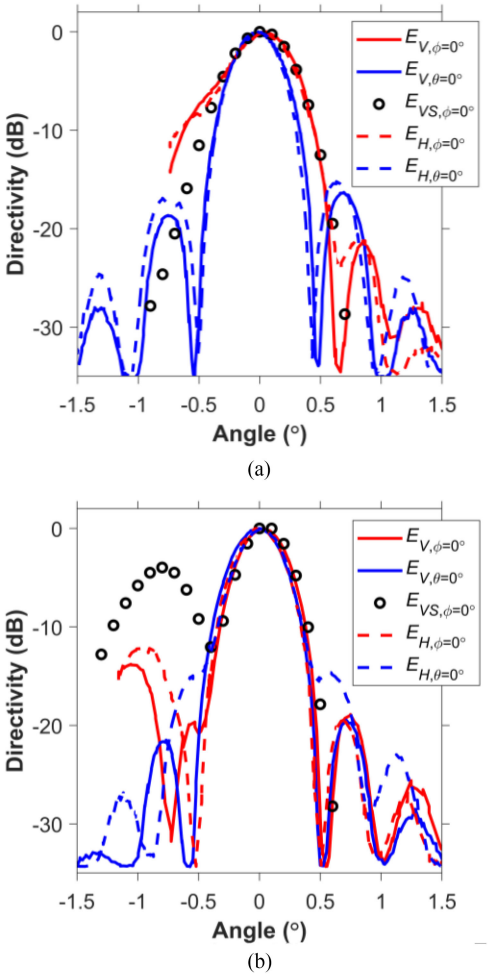


**FIGURE 17.** Vertical and horizontal polarized radiation patterns in the azimuth ($\theta = 0°$) and elevation ($\phi = 0°$) planes for receiver heights of (a) 5.5 m and (b) 11 m. Simulated results $E_{VS,\phi=0°}$ accounting for surface topography closely match the main beam shape in the elevation plane.

delivered wirelessly to a receiver at >1 km standoff with excellent RF-to-DC conversion efficiency, (iii) overvoltage protection circuits for rectenna arrays, and (iv) a second demonstration at higher average power driving an LED display.

### *A. BEAM CHARACTERIZATION*

Fig. 16 illustrates two experimental setups used to characterize the beam produced by the transmitter shown in Fig. 3. In the first setup, shown in Fig. 16a, a 100-kW pulsed power amplifier (PA) feeds the 5.4-m reflector antenna. The connection between the PA and reflector feed is WR-90 rectangular waveguide. A calibrated horn with 10.95 dBi gain at 9.73 GHz samples the power density at 1046-m standoff from the reflector. The reflector can scan in azimuth $\phi$ and elevation $\theta$, while the horn can translate in $x$ and $y$ in the plane of the receive aperture. Identical LadyBug LB680A power meters sample the power at both sites. In the second setup, shown in Fig. 16b, the link is reversed so that a 20-W continuous wave (CW) PA drives the horn antenna, and the reflector receives the power. Since the antenna directivities and terrain scattering are identical in both setups, cross checking between the two approaches makes it possible to identify and eliminate errors in deembedding system losses.

Measuring the radiation pattern of the reflector antenna at multiple heights on the receive tower confirms the impact of terrain effects on the beam shape. Fig. 17 shows the azimuth ($\theta = 0°$) and elevation ($\phi = 0°$) cuts of the reflector's radiation pattern when the antennas are oriented for both vertical ($E_V$) and horizontal ($E_H$) polarization measured using the setup in Fig. 16a. The reflector is boresighted to the horn at ($h_{RX} + \Delta h$ ) = 5.5 m and 11.0 m in Figs. 17a and 17b, respectively. For the elevation scans at the lower horn height, the reflector's range of travel is limited for elevations angles $\theta < -0.75°$. The measured radiation patterns for vertical and horizontal polarization match closely, as expected for very low grazing angles [23]. The parabolic equation simulation for the designed source distribution oriented for vertical polarization in the $\phi = 0°$ plane ($E_{VS,\ \phi=o°}$) shows excellent agreement with the measured main beam shape for both vertical and horizontal polarizations; outside the main beam, a large side lobe predicted in Fig. 17b is much reduced in experimental results. For concision, only vertically polarized results are illustrated in the remaining figures and tables of this paper.

**TABLE 1. Comparison Between Measured, Simulated and Optimal Values for the Half-Power Beam Width (HPBW)**

| Pattern Cut | HPBW at $h_{RX} = 5.5$ m | HPBW at $h_{RX} = 11$ m | HPBW in free space |
|---|---|---|---|
| $E_{V,\phi=0°}$ | 0.50 | 0.40 | ---- |
| $E_{V,\theta=0°}$ | 0.40 | 0.42 | ---- |
| $E_{VS,\phi=0°}$ | 0.51 | 0.41 | 0.40 |

Measured quantities appear in green text. For simplicity, only vertically polarized results are shown.

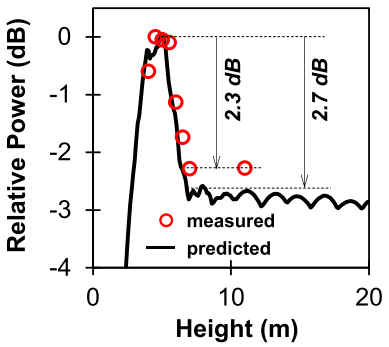


**FIGURE 18. Measured and simulated relative power density vs. receiver height, confirming the increase in power due to the ground bounce effect.**

Table 1 compares the measured half power beam width (HPBW) with simulated values for the designed aperture distribution $E_{VS,\ \phi=0°}$. Measured HPBW matches closely with simulated HPBW in the $\phi = 0°$ plane and with free space HPBW in the $\theta = 0°$ plane.

It is possible to determine the optimal receiver height at 1046 m standoff from the reflector by varying the height of the horn, boresighting the horn and reflector at each height, and measuring received power. Fig. 18 compares the result of this experiment with simulation. A sharp increase in received power is evident in the 4.5–5.5 m range, as predicted by simulation. The measured enhancement due to "ground bounce" is 2.3 dB, which although slightly less than the predicted value of 2.7 dB, nonetheless confirms the importance of terrain scattering in the design of terrestrial power beaming links.

Fig. 19 compares the measured radiation pattern determined via scanning over a ±0.24° range in azimuth $\phi$ and elevation $\theta$ with the measured power intensity determined by varying $x$-$y$ position in the receive aperture over a ±1.5 m range. Fig. 19a and b show projected coordinates in the $x$-$y$ and $\phi$-$\theta$ dimensions, respectively, for comparison. Increased variation in power density vs. height is clear in Fig. 19b, as predicted from the results in Fig. 18 – confirming the importance of spatial sampling of the received field for the accurate determination of the incident power at the receive aperture. The peak power density is 1643 W/m$^2$.

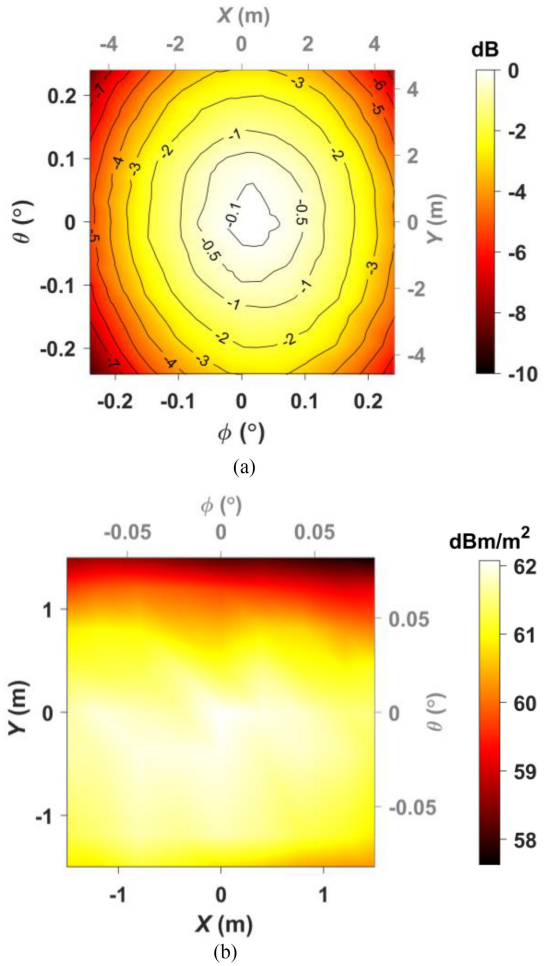


**FIGURE 19. (a) Measured radiation pattern of the focused beam pattern using the setup in Fig. 16a, with projected coordinates in the $x$-$y$ plane. (b) Map of power density in the receive plane using the setup in Fig. 16b, with projected coordinates in the $\phi$-$\theta$ plane.**

### B. POWER TRANSFER

The transmitter in Fig. 3 is next used to beam power to the rectenna array shown in Fig. 5b. The rectenna array is centered at $(h_{RX} + \Delta h) = 5.5$ m based on mechanical considerations at the test site. Reviewing manufacturer's specifications for the maximum input power of the MA4E1317, the estimated maximum power handling of the rectenna array (neglecting losses in the microstrip antenna and matching network) is 444 W/m$^2$. As shown in Fig. 20, the linearly actuated feed in Fig. 3b can defocus the beam, providing a mechanism for controlling power density over a >10 dB range. Fig. 21 illustrates the power density at the plane of the rectenna array with the feed defocused at a displacement of 40 mm. During this test condition, the received power density shown in Fig. 21b is additionally reduced by a 2 x 1.3 x 1.7 m steel dumpster abandoned directly in the line of sight of the transmitter at 262 m standoff. This notwithstanding, the transmitter provides reasonably uniform power density at the plane of the rectenna with 552 W/m$^2$ power density at the center of the target area. The total power integrated over the aperture of the rectenna

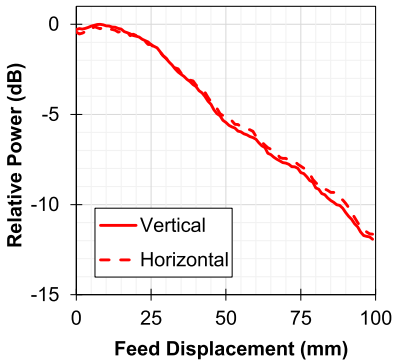


**FIGURE 20.** Variation in power at the center of the receive aperture, measured using the setup in Fig. 16a, for different feed displacements at the reflector antenna. Controlling the feed displacement defocuses the beam, making it possible to control the power density incident on the rectenna.

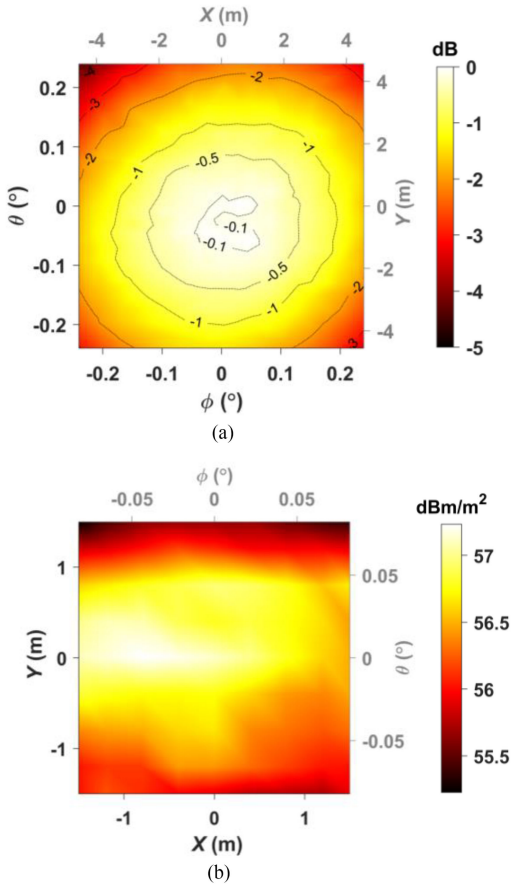


**FIGURE 21.** (a) Measured radiation pattern of the defocused beam pattern using the setup in Fig. 16a, with projected coordinates in the *x*-*y* plane. (b) Map of power density in the receive plane using the setup in Fig. 16b, with projected coordinates in the $\phi$-$\theta$ plane. Power density in the center of the *x*-*y* plane is 552 W/m$^2$.

array at this 40 mm feed displacement is 2265 W. Comparing measured gain of the transmitter reflector antenna (including the loss of the feed horn and the effect of terrain scattering) between the two setups in Fig. 16 shows agreement within 0.20 dB – indicating that system losses are well controlled.

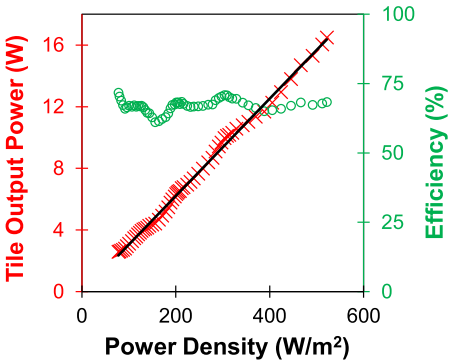


**FIGURE 22.** Output power and efficiency for a single rectenna tile, shown in Fig. 4b, vs. incident power density. The black line represents a linear fit of the data.

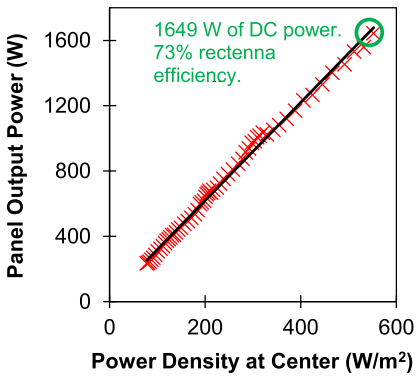


**FIGURE 23.** Output power and efficiency for the complete rectenna array shown in Fig. 5c vs. incident power density. The black line represents a linear fit of the data.

An individual rectenna tile is mounted in the center of the target area as the incident power density sweeps over a 98 to 524 W/m$^2$ range. Fig. 22 shows the rectenna's measured output power across a 180 Ω load and the corresponding RF-to-DC conversion efficiency calculated by dividing the output power by the total power incident on the surface of the rectenna tile. Although not statistically representative, 16.5 W output power is achieved at a power density of 522 W/m$^2$, corresponding to an RF-to-DC conversion efficiency of 68%. A peak efficiency of 71% is achieved at a power density of 304 W/m$^2$.

Repeating this experiment for the entire rectenna array achieves 1649 W output power delivered to a 30-Ω resistor, as shown in Fig. 23, for the incident power density shown in Fig. 21b. Integrating this power density over the rectenna aperture yields a total of 2265 W incident power. The corresponding RF-to-DC conversion efficiency is 73%. This result compares well with the state of the art reported to date at X band [1]. Repeating this experiment with the transmitter and receiver oriented for horizontal polarization (not shown in the figure) achieves 1581 W of output power at an illumination condition yielding 2229 W of incident RF power, which corresponds to an RF-to-DC conversion efficiency of 71%. Note that sources of experimental error in this efficiency calculation could include the use of a calibrated horn to map the received

power density in Fig. 21b, which may respond differently to multipath scattering in comparison to the microstrip patch elements in the rectenna.

### C. OVERVOLTAGE PROTECTION

Overvoltage protection devices such as transient voltage suppression (TVS) diodes and Zener diodes are sometimes used [28], [29] to limit rectenna output voltage in the event that the rectenna receives RF power while no DC load is connected. No information, however, is available on whether such protection devices also enhance the survivability of large rectenna arrays to excess power density encountered during ordinary operation – i.e., when a DC load is connected.

Fundamentally, solid-state device failure is accelerated by three factors: excessive voltage, excessive current, and excessive temperature. It is hypothesized that constraining one of these factors (voltage) could increase the margin of survivability as another of the factors (current) increases with increasing incident power density.

In the case of the MA4E1317 Schottky diode used in this paper, the manufacturer is unable to provide reliability information beyond the 20 dBm maximum RF input power specification. However, since this paper's variable-focus transmitter can provide a controllable uniform high power density over a large receive aperture, it is possible to experimentally evaluate the impact of overvoltage protection on rectenna survivability in a realistic system test. To do this, each of the four rectenna quadrants shown in Fig. 4 is mounted, one at a time, on the receive tower at the center of the target area. Individual 1 $\mu$s pulses of incrementally increasing power are transmitted at each quadrant until damage/degradation is observed using an oscilloscope to monitor the rectenna output.

The first quadrant in this test series has no overvoltage protection. The second quadrant uses four 53-V TVS diodes (STMicroelectronics 1.5KE62A) to protect 4 groups of 6 rectenna tiles within the quadrant. The third quadrant is protected by four 56-V Zener diodes (ON Semiconductor 1N5370BG). The fourth quadrant is protected by shorting the rectenna output; after each high power pulse, the short is removed and the output is checked for degradation at a nominal power density. As shown in Fig. 24, the unprotected rectenna quadrant reaches an output power of 672 W before incurring damage, indicating that the output power achieved of the full array could have pushed significantly beyond 1.6 kW to as high as 2.7 kW before destruction. While the TVS diode provides little improvement over the unprotected array, the array protected by the Zener diode fails at 1.1 dB higher input power density. The 1.7 dB increase in power handling for the array protected by the short circuit establishes an upper bound on the performance of overvoltage protection devices, from the standpoint of response time and parasitic resistance.

It can be argued that the results in Fig. 24 are statistically significant because (*i*) each quadrant contains 4872 diodes, (*ii*) the Schottky diodes in large rectenna arrays tend to "fail safe", degrading gracefully as an ensemble until severe failure is reached [30]. Given the duality between power amplifiers and rectifiers [31], a >1 dB increase in RF power handling can be understood as a substantial improvement in survivability.

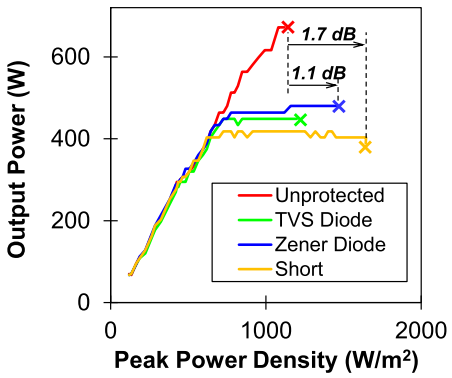


**FIGURE 24.** Test to destruction for the four quadrants of the rectenna array comparing the effectiveness of the TVS diode, Zener diode, and short circuit protection for improving input RF power handling.

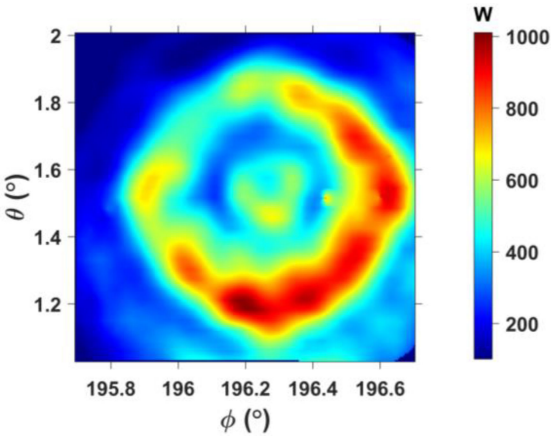


**FIGURE 25.** Optimizing transmitter alignment to the rectenna array shows a maximum of 1030 W at $\phi = 196.2°$ and $\theta = 1.2°$. The oculus pattern results from the fact that the phase profile of the HUSIR transmitter is fixed.

### D. LED DEMONSTRATION

The HUSIR transmitter and rectenna array shown in Fig. 7 are used for a power beaming demonstration at higher duty factor. Since HUSIR's Cassegrain feed and subreflector are immobile and focused at the far field, and since the 1.1 km link distance is only 1.2% of HUSIR's far field distance, the field incident at the plane of the rectenna is complex and irregular. To optimize the alignment, the transmitter scans about boresight $\pm 1°$ in azimuth and elevation while monitoring the rectenna output power delivered to a 30 Ω load. As shown in Fig. 25, a maximum of 1030 W appears at $\phi = 196.2°$ and $\theta = 1.2°$. The oculus power distribution in this figure corresponds to simulated predictions.

A light emitting diode (LED) display is mounted beneath the rectenna array at a 30° angle from vertical, allowing visibility from the ground and from the air. The array is constructed using KXZM B08H51WGRN green LED strips with adhesive backing. Each 25 mm segment of the strips contains

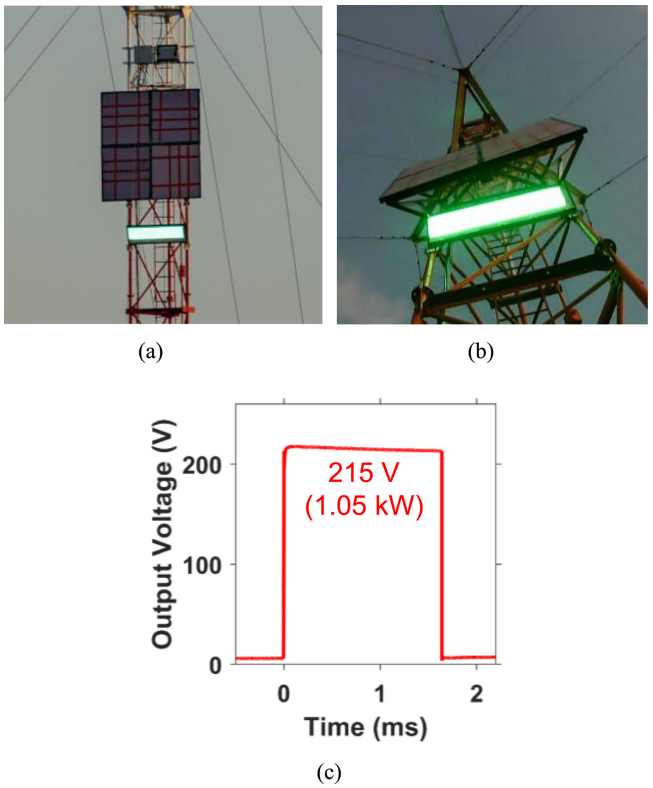


**FIGURE 26.** **Demonstration using the MIT HUSIR transmitter for higher average power. (a) LED display. (b) Screenshot of a video available online at https://ieeexplore.ieee.org/document/9662403/media#media. Flickering in the video is an artifact of the camera sampling rate and not visible to the human eye. The images are intentionally dimmed since the brightness is excessive for the naked eye. (c) Output voltage and power of the rectenna driving the LED load.**

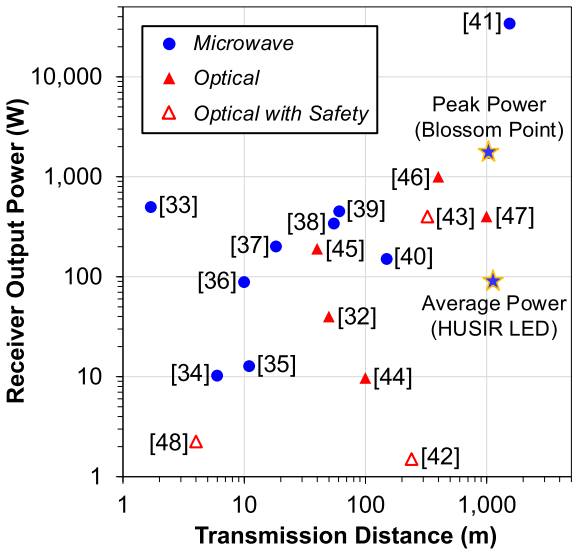


**FIGURE 27.** **Comparison of this work to prior documented results for received power vs. transmission distance.**

three 12-V LEDs and a 121 Ω current limiting resistor. 12 groups of 2 parallel-connected 1.1-m strips combine in series to create a 0.3 x 1.1 m display. The photograph in Fig. 26a and video in Fig. 26b shows the display in operation – with the brightness dimmed in the video since the brightness is excessive for the naked eye. Referring to Fig. 26c, the pulse width is 1.638 ms, repeated at a 50 Hz rate. Averaging 11 pulses and computing the average voltage within the pulse shows 215 V, which corresponds to 1.05 kW dissipated in the light display. In continuous operation (not possible here), the LED voltage and power would drop to 213 V and 1.03 W, respectively, based on the settled value at the end of the pulse. Using an identical power sensor and calibrated antenna as in Fig. 16a, the incident power at the rectenna is estimated via $\phi$-$\theta$ scanning as 1733 W, corresponding to 61% RF-to-DC conversion efficiency. Since this efficiency includes at least 0.3 dB of polarization mismatch loss between HUSIR and the rectenna, this calculated efficiency is considered more approximate than the results reported in Section 4-B.

### *E. COMPARISON WITH PRIOR ART*

Fig. 27 compares the demonstration in this paper with prior documented results [32]–[48] for rectenna output power vs. transmission distance. Both microwave and optical power beaming results are shown. The highest result recorded result is W. Brown's 2.39-GHz demonstration of 34 kW received at 1.55 km. The 9.7 and 10.5 GHz demonstrations in this work exceed all other prior microwave results in terms of transmission distance.

Table 2 summarizes the results in this paper in terms of total RF power input to the transmit antenna and total power received at the output of the rectenna. The overall link efficiency (i.e., the ratio of rectenna output power to the RF power input to the transmitter) demonstrated experimentally is 1.8%. The major limitation in this rapid demonstration is the discrepancy between the transmitter's peak RF power and the limited power handling capability of commercial Schottky diodes, which made it necessary to de-focus the beam in order to limit power density at the rectenna to the 500–600 W/m$^2$ range. Table 2 therefore provides case studies projecting potential extensions of this work to higher levels of performance. Case B reduces the RF transmit power by 4.4 dB so that the beam can be fully focused on the rectenna without destruction, increasing link efficiency to 5%. Cases C and D further increase link efficiency to 25% and 44%, respectively, by using larger rectennas. Cases E and F are the same as C and D, but with a uniform aperture distribution (i.e., 0 dB amplitude taper) so that the required rectenna sizes are less. Although a uniform amplitude distribution is impossible with a reflector, Cases E and F show what would be reasonably achievable with a spatially combined architecture; the estimated output power and efficiency in these cases is conservative since the same transmit efficiency is used as for Cases A, B, C, and D (i.e., aperture efficiency corresponding to 17 dB amplitude taper conditions).

**TABLE 2. Summary of Results and Projected Extension to Higher Performance**

| PARAMETER | THIS WORK | CASE B | CASE C | CASE D | CASE E | CASE F |
|---|---|---|---|---|---|---|
| RF Input to TX Antenna | 91.2 kW | 33.0 kW | 30.6 kW | 30.6 kW | 30.6 kW | 30.6 kW |
| Aperture Taper | 17 dB | 17 dB | 17 dB | 17 dB | 0 dB | 0 dB |
| Rectenna Area | 4.49 $m^2$ | 4.49 $m^2$ | 30.2 $m^2$ | 101 $m^2$ | 18.6 $m^2$ | 53.0 $m^2$ |
| Incident Power on Rectenna | 2.27 kW | 2.27 kW | 15.3 kW | 27.6 kW | 15.3 kW | 27.6 kW |
| Rectenna Output Power | 1.65 kW | 1.65 kW | 8.11 kW | 14.6 kW | 8.11 kW | 14.6 kW |
| RF-DC Conversion Efficiency Across Link | 1.8% | 5.0% | 25% | 44% | 25% | 44% |

In Case B, the RF transmit power is reduced so that the beam can be fully focused on the rectenna without destruction. Cases C and D are the same as Case B, but with larger rectenna arrays. In Cases E and F, the aperture distribution is forced to be uniform for comparison.

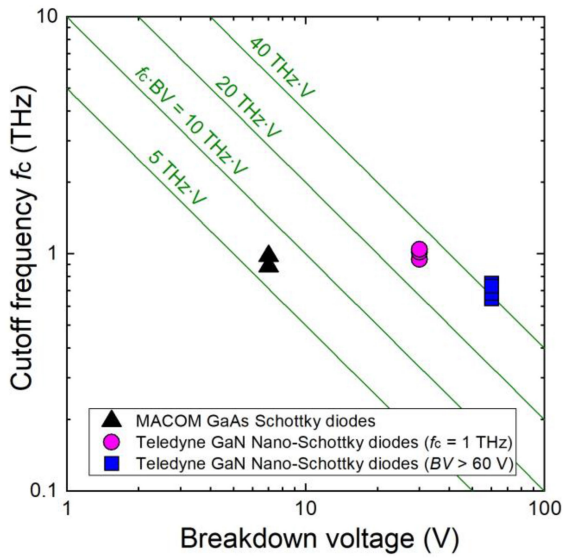


**FIGURE 28. Comparison of GaN nano-Schottky diodes to the best commercially available GaAs Schottky diodes (MACOM MA4E1317) used in this paper. From [52].**

## V. RECOMMENDATIONS FOR ADDITIONAL RESEARCH

This paper has established the technical practicality of microwave power beaming across terrain. Key steps needed to mature the technology for operational use include:

***1. Scalable Spatially Combined Microwave Sources:*** The reflector antenna used in this paper is low cost and effective, but there is a drawback. A reflector has a single input for microwave power, and unitary microwave power sources in the >10 kW range are typically pulsed. Continuous sources at >10 kW are rare, expensive, and difficult to maintain. A more realistic alternative is to spatially combine the power from numerous smaller microwave sources, as in active electronically scanned arrays (AESAs) [49]. Additional benefits of spatial power combining are scalability to the application/distance and the possibility of *in situ* optimization of the aperture's amplitude and phase distribution in the presence of terrain. Unfortunately, little work has been done to develop spatially combined microwave sources that are both high power and low cost. At S band, researchers are beginning to consider both vacuum [50] and solid state [51] approaches, but challenges of size, weight, power, and cost are apparent.

***2. High Power Handling Schottky Diodes:*** Brown's historic demonstration in [41] used custom S band Schottky diode technology to achieve high power handling and high rectenna efficiency. Since this technology no longer exists, alternatives are needed to attain or exceed that level of performance. Although GaN transistors can be used to make create high power microwave rectifiers [28], additional performance is expected using solid-state devices optimized for the rectifier application. Recent results in GaN nano-Schottky diode technology from Teledyne Scientific Company [52], presented in Fig. 28 and compared with the MACOM MA4E1317 GaAs Schottky diodes used in this work, show major improvements in breakdown voltage. If productized, such devices could lead to records in rectenna output power at frequencies >10 GHz.

***3. Rectenna Power Management Subsystems***. Although implementation of rectenna power management and dc-dc conversion are well established for battery charging and low power applications [53]–[55], considerable work is needed to integrate rectennas into general purpose microgrids. This should be compared to the high level of development for photovoltaic power management systems [56]. In the case of high efficiency rectennas, there are special design considerations, such as the need to present an optimal resistive load at the rectenna output [29] for optimal efficiency.

## VI. CONCLUSION

This paper presented several important technical demonstrations. 1.6 kW of electrical power was delivered at >1 km standoff from a 5.4-m-diameter X band transmitter. A 4 $m^2$ rectenna produced the 1.6 kW of output power at a 73% RF-to-DC conversion efficiency, which exceeds the current state of the art at X band. A 2.3 dB enhancement in power density at the target site was achieved by deliberate exploitation of a ground bounce over cluttered, irregular terrain. Overvoltage protection techniques increased power handling by >1 dB. In addition, 1.2 kW of electrical power was delivered to an LED display at 1.1 km. Technical measures to extend these demonstrations to higher levels of power and performance were also provided.

A key finding was the need to consider and exploit the effects of microwave propagation across terrain in terrestrial microwave power beaming applications. As a result of these demonstrations, the feasibility of transmitting microwave power over terrain has been established. Recommendations for additional research were provided to mature the technology for operational use.

## ACKNOWLEDGMENT

The authors wish to thank R. Darling of the Office of the Undersecretary of Defense for Acquisition and Sustainment, Arlington, VA, USA for guidance and support; J. Winter and M. Self at Air Force Research Laboratory, Albuquerque, NM, for initiating valuable technical interactions that set the stage for this work; M. Walder of Naval Research Laboratory, Washington, DC, USA for oversight of this program; and LT S. Cowart, U.S. Navy, for insight on defense applications.

These experimental demonstrations would not have been possible without invaluable, timely technical assistance from R. Benevente, L. Larose, and S. Dilbeck of Naval Research Laboratory, Blossom Point, MD, USA; D. Kaufman of Envisioneering, Inc., Alexandria, VA, USA; G. Flynn and A. Melchior of Lakenheath Electronics, Bethesda, MD, USA; and M. Abouzahra, T. Hiett, and the technical staff at Lincoln Laboratory, Westford, MA, USA; and G. Hatzilias and the technical staff at Engent, Inc., Norcross, GA, USA.

The authors also thank Prof. O. Ozgun of Hacettepe University, Ankara, Turkey for generously providing editable MATLAB scripts for the core components of the PETOOL propagation simulator.

## REFERENCES

[1] C. T. Rodenbeck *et al.*, "Microwave and millimeter wave power beaming," *IEEE J. Microwaves*, vol. 1, no. 1, pp. 229–259, Jan. 2021, doi: 10.1109/JMW.2020.3033992.

[2] "Opinion: Electricity can be transmitted through the air," *Ed.ial Board, Economist*, Feb. 25, 2021. [Online]. Available: https://www.economist.com/science-and-technology/2021/02/25/electricity-can-be-transmitted-through-the-air

[3] L. Okwatch, "How far are we from wireless electricity?," *Medium*, Dec. 6, 2020. [Online]. Available: https://medium.com/predict/how-far-are-we-from-wireless-electricity-94dbd48529a4

[4] E. Cavallaro, "Researchers transmit energy with laser in historic power beaming demonstration," *Physics*, Oct. 29, 2019. [Online]. Available: https://phys.org/news/2019-10-transmit-energy-laser-historic-power-beaming.html

[5] Larson, "Serious power transmission without wires is closer than you think," *Power Mag.*, Apr. 2021. [Online]. Available: https://www.powermag.com/serious-power-transmission-without-wires-is-closer-than-you-think/

[6] D. Wagman, "Emrod chases the dream of utility-scale wireless power transmission," *IEEE Spectr.*, Aug. 2020. [Online]. Available: https://spectrum.ieee.org/emrod-chases-the-dream-of-utilityscale-wireless-power-transmission

[7] M. Williams, "Exploring the Moon's shadowed regions using beamed energy," *Universe Today*, Mar. 26, 2021. [Online]. Available: https://www.universetoday.com/150565/exploring-the-moons-shadowed-regions-using-beamed-energy/

[8] W. C. Brown, "The history of power transmission by radio waves," *IEEE Trans. Microw. Theory Techn.*, vol. 32, no. 9, pp. 1230–1242, Sep. 1984, doi: 10.1109/TMTT.1984.1132833.

[9] T. Nishioka and S. Yano, "Mitsubishi Heavy takes step toward long-distance wireless power," in *Nikkei Asian Review*, Chiyoda City, Tokyo, Japan: Mitsubishi Heavy Industries, Mar. 2015.

[10] U.S. Geological Survey 3D Elevation Program. [Online]. Available: https://www.usgs.gov/core-science-systems/ngp/3dep

[11] U.S. Geological Survey, "USGS 1/3 arc second n39w078," Jun. 10, 2021. [Online]. Available: https://www.sciencebase.gov/catalog/item/60c44002d34e86b93898fb5b

[12] U.S. Geological Survey, "What is the vertical accuracy of the 3D elevation program (3DEP) DEMs?." Accessed: Sep. 20, 2021. [Online]. Available: https://www.usgs.gov/faqs/what-vertical-accuracy-3d-elevation-program-3dep-dems?qt-news_science_products=0#qt-news_science_products

[13] T. Chu, "A note on simulating Fraunhofer radiation patterns in the Fresnel region," *IEEE Trans. Antennas Propag.*, vol. 19, no. 5, pp. 691–692, Sep. 1971, doi: 10.1109/TAP.1971.1140000.

[14] P. Mousavi, L. Shafai, B. Veidt, and P. Dewdney, "Feed-reflector design for large adaptive reflector antenna (LAR)," *IEEE Trans. Antennas Propag.*, vol. 49, no. 8, pp. 1142–1154, Aug. 2001, doi: 10.1109/8.943309.

[15] R. W. Bickmore, "On focusing electromagnetic radiators," *Can. J. Phys.*, vol. 35, no. 11, pp. 1292–1298, 1957.

[16] R. W. Bickmore, "Fraunhofer pattern measurement in the Fresnel region," *Can. J. Phys.*, vol. 35, no. 11, pp. 1299–1308, 1957.

[17] M. G. Czerwinski and J. M. Usoff, "Development of the haystack ultrawideband satellite imaging radar," *Lincoln Lab. J.*, vol. 21, no. 1, pp. 28–34, 2014.

[18] S. Silver, *Microwave Antenna Theory and Design*. New York, NY, USA: McGraw-Hill, 1949.

[19] K. Fujimoto, *Mobile Antenna Systems Handbook*, 3rd ed. Norwood, MA, USA: Artech House, 2008.

[20] T. A. Milligan, *Modern Antenna Design*, 2nd ed. New York, NY, USA: Wiley, 2005.

[21] O. Ozgun *et al.*, "PETOOL v2.0: Parabolic equation toolbox with evaporation duct models and real environment data," *Comput. Phys. Commun.*, vol. 256, 2020.

[22] O. Ozgun, G. Apaydin, M. Kuzuoglu, and L. Sevgi, "PETOOL: MATLAB-based one-way and two-way split-step parabolic equation tool for radiowave propagation over variable terrain," *Comput. Phys. Commun.*, vol. 182, pp. 2638–2654, 2011.

[23] M. Dolukhanov, *Propagation of Radio Waves*. Moscow, Russia: Mir Publishers, 1971.

[24] International Commission on Non-Ionizing Radiation Protection (ICNIRP), "ICNIRP guidelines for limiting exposure to electromagnetic fields (100 kHz to 300 GHz)," *Health Phys.*, vol. 118, no. 5, pp. 483–524, 2020.

[25] *IEEE Standard for Safety Levels With Respect to Human Exposure to Electric, Magnetic, and Electromagnetic Fields, 0 Hz to 300 GHz*, IEEE Std C95.1-2019, Oct. 2019.

[26] *IEEE Standard for Military Workplaces – Force Health Protection Regarding Personnel Exposure to Electric, Magnetic, and ElectRomagnetic Fields, 0 Hz to 300 GHz*, IEEE Std C95.1-2345-2014, May 2014.

[27] T. A. Cott, "RF radiation environment over Millstone hill," MIT Lincoln Laboratory, Tech. Rep. 1141, Dec. 2019.

[28] C. Walsh, S. Rondineau, M. Jankovic, G. Zhao, and Z. Popovic, "A conformal 10 GHz rectenna for wireless powering of piezoelectric sensor electronics," in *Proc. IEEE Int. Microw. Symp.*, 2005, pp. 143–146, doi: 10.1109/MWSYM.2005.1516543.
[29] B. B. Tierney, C. T. Rodenbeck, M. G. Parent, and A. P. Self, "Scalable, high-sensitivity X-band rectenna array for the demonstration of space-to-earth power beaming," *IEEE Access*, vol. 9, pp. 27897–27907, 2021, doi: 10.1109/ACCESS.2021.3057020.
[30] W. C. Brown, "The history of the development of the rectenna," *Sol. Power Satell. Microw. Power Transmiss. Reception*, vol. 2141, 1980, Art. no. 271.
[31] M. Litchfield, S. Schafer, T. Reveyrand, and Z. Popovic, "High-efficiency X-band MMIC GaN power amplifiers operating as rectifiers," in *Proc IEEE Int. Microw. Symp.*, 2014, pp. 1–4, doi: 10.1109/MWSYM.2014.6848394.
[32] P. N. Kawashima and K. Takeda, "Laser energy transmission for a wireless energy supply to robots," in *Robotics and Automation in Construction*. Greater Noida, Uttar Pradesh, India: Intech Digital Technology India Pvt. Ltd., Oct. 2008, doi: 10.5772/6194.
[33] R. M. Dickinson and W. C. Brown, "Radiated microwave power transmission system efficiency measurements," NASA Tech. Memo 33-727, May 1975.
[34] K. D. Song *et al.*, "Preliminary operational aspects of microwave-powered airship drone," *Int. J. Micro Air Veh.*, Jan. 2019, doi: 10.1177/1756829319861368.
[35] B. Duan, "On new developments of space solar power station (SSPS) of China," in *Proc. 36th Int. Space Develop. Conf.*, 2017, pp. 1–80.
[36] N. Shinohara, "Beam control technologies with a high-efficiency phased array for microwave power transmission in Japan," *Proc. IEEE*, vol. 101, no. 6, pp. 1448–1463, Jun. 2013.
[37] W. C. Brown, "The history of the development of the rectenna," in *SPS Microwave Systems Workshop*. Houston, TX, USA: Lyndon B. Johnson Space Center, Jan. 1980.
[38] "Ground demonstration testing of microwave wireless power transmission," *JAXA Res. Develop. Directorate*. Accessed: Jul. 9, 2020. [Online]. Available: http://www.kenkai.jaxa.jp/eng/research/ssps/150301.html
[39] R. M. Dickinson and O. Maynard, "Ground based wireless and wired power transmission cost comparison," in *Proc. Int. Energy Convers. Eng. Conf*, 1999, Art. no. 20060034148. Accessed: Apr. 25, 2020. [Online]. Available: http://hdl.handle.net/2014/17841
[40] J. J. Schlesak, A. Alden, and T. Ohno, "A microwave powered high altitude platform," in *Proc. IEEE Int. Microw. Symp.*, no. 1, 1988, pp. 283–286.
[41] R. M. Dickinson, "Wireless power transmission technology state of the art the first bill brown lecture," *Acta Astronautica*, vol. 53, no. 4, pp. 561–570, 2003. [Online]. Available: http://dx.doi.org/10.1016/S0094-5765(03)80017-6
[42] "Transmitting power without wires," *Bang Goes the Theory - Series 6, Episode 5*. College Park, MD, USA: BBC One, May 22, 2012. [Online]. Available: https://www.bbc.co.uk/programmes/p00yjt99
[43] T. J. Nugent Jr., D. Bashford, T. Bashford, T. J. Sayles, and A. Hay, "Long-range, integrated, safe laser power beaming demonstration," in *Proc. Opt. Wireless Fiber Power Transmiss. Conf.*, 2020, pp. 12–13.
[44] T. He *et al.*, "High-power high-efficiency laser power transmission at 100 m using optimized multi-cell gaas converter," *Chin. Phys. Lett.*, vol. 31, no. 10, pp. 1042031–1042035, 2014.
[45] R. Akiba, K. Miura, M. Kinada, H. Matsumoto, and N. Kaya, "ISY-METS rocket experiment," *Inst. Space Astronautical Sci. Rep.*, 1993.
[46] T. Nugent, "Review of laser power beaming demonstrations by powerlight technologies (formerly lasermotive)," in *Proc. Directed Energy Sci. Technol. Symp.*, 2018, pp. 1–48.
[47] T. Talbert, "NASA - LaserMotive LLC wins prize in power beaming challenge," Accessed: May 1, 2020. [Online]. Available: https://www.nasa.gov/offices/oct/early_stage_innovation/centennial_challenges/cc_pb_feature_11_10_09.html
[48] [Online]. Available: https://wi-charge.com/product_category/reference-integrations
[49] M. Yeary, R. Palmer, C. Fulton, J. Salazar, and H. Sigmarsson, "Update on an S-band all-digital mobile phased array radar," in *Proc. IEEE Radar Conf.,* 2021, pp. 1–4, doi: 10.1109/RadarConf2147009.2021.9455287.
[50] X. Chen, B. Yang, N. Shinohara, and C. Liu, "Low-noise dual-way magnetron power-combining system using an asymmetric H-plane tee and closed-loop phase compensation," *IEEE Trans. Microw. Theory Techn.*, vol. 69, no. 4, pp. 2267–2278, Apr. 2021, doi: 10.1109/TMTT.2021.3056550.
[51] S. Mihara *et al.*, "The plan of microwave power transmission development for SSPS and its industry application," in *Proc. Asia-Pacific Microw. Conf.*, 2018, pp. 443–445.
[52] Communication from K. Shinohara. Thousand Oaks, CA, USA: Teledyne Scientific.
[53] B. Strassner and K. Chang, "Passive 5.8-GHz radio-frequency identification tag for monitoring oil drill pipe," *IEEE Trans. Microw. Theory Techn.*, vol. 51, no. 2, pp. 356–363, Feb. 2003, doi: 10.1109/TMTT.2002.807832.
[54] J. A. Hagerty, F. B. Helmbrecht, W. H. McCalpin, R. Zane, and Z. B. Popovic, "Recycling ambient microwave energy with broad-band rectenna arrays," *IEEE Trans. Microw. Theory Techn.*, vol. 52, no. 3, pp. 1014–1024, Mar. 2004, doi: 10.1109/TMTT.2004.823585.
[55] T. Paing, J. Shin, R. Zane, and Z. Popovic, "Resistor emulation approach to low-power RF energy harvesting," *IEEE Trans. Power Electron.*, vol. 23, no. 3, pp. 1494–1501, May 2008, doi: 10.1109/TPEL.2008.921167.
[56] S. Bacha, D. Picault, B. Burger, I. Etxeberria-Otadui, and J. Martins, "Photovoltaics in microgrids: An overview of grid integration and energy management aspects," *IEEE Ind. Electron. Mag,* vol. 9, no. 1, pp. 33–46, Mar. 2015, doi: 10.1109/MIE.2014.2366499.

**CHRISTOPHER T. RODENBECK** (Fellow, IEEE) received the B.S. (*summa cum laude*), M.S., and Ph.D. degrees in electrical engineering from Texas A&M University, College Station, TX, USA, in 1999, 2001, and 2004, respectively. His graduate studies were supported by fellowships from NASA, the State of Texas "to advance the state of the art in telecommunications," Texas A&M, and TXTEC in addition to grants from Raytheon, TriQuint Semiconductor, the Office of the Secretary of Defense, NASA Jet Propulsion Lab, NASA Glenn Research Center, and U.S. Army Space Command.

He is currently an Office Head with U.S. Naval Research Laboratory (NRL), Washington, DC, USA, where he heads the Radar Division's Advanced Concepts Group. He leads multiple research programs in microwave power beaming and is the Principal Investigator of Air Force Research Laboratory's Arachne power beaming spacecraft. His programs with NRL have resulted in the development of multiple first-in-class millimeter-wave airborne radar systems for the U.S. Navy and Department of Defense. From 2004 to 2014, he led a multidisciplinary advanced/exploratory technology development program for radar and sensor applications with Sandia National Laboratories, Albuquerque, NM, USA. The success of this work was twice the subject of Congressional testimony by Sandia's President. He has authored or coauthored 42 refereed journal papers, 24 patents and patent applications, 31 conference papers, and 29 government reports. He is responsible for numerous radar technology innovations in short- and long-range airborne millimeter wave radar systems and antennas, ultrawideband pulsed power amplifiers, CMOS radiation hardening by design, highly sensitive radar digitizers, advanced RF modules, electro-optical inspection of RF circuits, solid-state device modeling, electrically small antennas, and software-defined fusion of radar and telemetry.

Dr. Rodenbeck was the recipient of the 2016 Texas A&M University Outstanding Early Career Professional Achievement Award from among more than 100 000 engineering alumni. He was the recipient of the IEEE MTT-S Outstanding Young Engineer Award in 2015, was the Principal Investigator for an R&D Program recipient of the prestigious 2012 NNSA Award of Excellence, Sandia Innovator Award in 2013, and Sandia internal citation for "Excellence in Radar Technology Leadership" in 2011. He was an Associate Editor for the *Encyclopedia of Electrical and Electronics Engineering* (New York, NY, USA: Wiley) from 2011 to 2020, and is currently the Editor-in-Chief of the *Encyclopedia of RF & Microwave Engineering,* 2nd ed. (New York, NY, USA: Wiley).

**BRIAN B. TIERNEY** (Member, IEEE) received the B.S. degree in electrical engineering from Kansas State University, Manhattan, KS, USA, in 2011, and the M.S.E. and Ph.D. degrees in electrical engineering from the University of Michigan, Ann Arbor, Ann Arbor, MI, USA, in 2014 and 2016, respectively.

Since 2016, he has been with Radar Division, U.S. Naval Research Laboratory, Washington, DC, USA. His current research interests include advanced radar concepts, microwave circuits, wireless power transfer, electromagnetic theory, and digital signal processing.

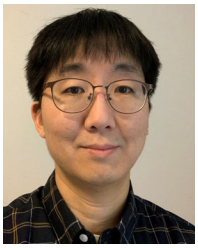

**JAMES PARK** received the Ph.D. degree in electrical and computer engineering from the Ohio State University, Columbus, OH, USA, in 2012. He is currently an Electronics Engineer with Radar Division, U.S. Naval Research Laboratory, Washington, DC, USA. Prior to this, he was with Air Force Research Laboratory, Sensors Directorate, where he researched on electromagnetic scattering signatures of target and clutter. His research interests include signal/image processing problems in radar and microwave remote sensing.

**MARK G. PARENT** received the B.S. degree in electrical engineering and the M.S. degree in physics from Michigan Technological University, Houghton, MI, USA, in 1982 and 1985, respectively.

He was with Northrup Grumman, Rolling Meadows, IL, USA, and since 1985 he has been with Radar Division, Naval Research Laboratory, where he is currently a Senior Staff Member. He has authored or coauthored numerous journal articles and conference papers and holds several patents. His research interests include optical beamforming, HF vector sensors, high isolation system development, RCS measurements, monopulse beamformers, low sidelobe corrugated horn designs and various other antenna related projects. He has also supported and developed numerous experimental field tests during his time at NRL.

**CHRISTOPHER B. DEPUMA** is currently an Electronics Engineer with the Spacecraft Electronics Branch of the U.S. Naval Research Laboratory (NRL), Washington, DC, USA, where he is the Program Manager of photovoltaic radiofrequency antenna module (PRAM). This experiment currently flying on the Air Force X-37B, is a prototype of a future Solar Power Satellite that aims to convert solar energy in space to a microwave transmission that can be sent back to earth for terrestrial use. He has also supported the DARPA-funded, NRL-led Robotic Servicing of Geosynchronous Satellites (RSGS) Program on tasks, including the environmental test campaign and harness design efforts. In addition to the previously mentioned space efforts, he leads demonstration activities for the Safe and Continuous Power Beaming – Microwave (SCOPE-M) Program.

**CHANDLER J. BAUDER** (Graduate Student Member, IEEE) received the B.S. degree (*summa cum laude*) in electrical engineering in 2018 from the University of Tennessee, Knoxville, TN, USA, where he is currently working toward the Ph.D. degree in electrical engineering.

Since May 2018, he has been a Graduate Research Assistant with the Department of Electrical Engineering and Computer Science, University of Tennessee Knoxville. He has worked on projects involving ground penetrating radar, microstrip filter design, radar and camera signal processing for vital sign detection, and multipactor breakdown simulation of RF components. In May 2021, he began working as an Intern with U.S. Naval Research Laboratory Radar Division's Advanced Concepts Group, on a project involving microwave power beaming. He was awarded the Gonzalez Family Award for Outstanding Electrical Engineering Junior in 2017. He was awarded the Chancellor's Award for Extraordinary Academic Achievement in 2018 and the Chancellor's Award for Extraordinary Professional Promise in 2019 and 2020.

**THOMAS J. PIZZILLO** joined U.S. Naval Research Laboratory, Washington, DC, USA, in January 2015, as the Head of Radar Analysis Branch. From 2013 to 2015, he was the Vice President of R&D with WM Robots LLC, a small business specializing in force protection and explosives detection sensors and robots. Prior to this, he has spent 25 years with Army Research Laboratory, where he led several programs related to radar and sensor phenomenology, including the JIEDDO-funded, IED detection technologies Experiment-Fix program responsible for assembling and leading a matrix team of government and contractor personnel in the technical assessment, experimental development, acquisition, and fielding of counter IED technologies. He has deep experience in DOD technology development and leads a team with world-class expertise in electromagnetics, antennas, ISR signal processing, and radar phenomenology.

**PAUL I. JAFFE** (Senior Member, IEEE) received the B.S. degree in electrical engineering from the University of Maryland, College Park, MD, USA, in 1996, the M.S. degree (with hons.) in electrical engineering from the Johns Hopkins University, Baltimore, MD, USA, in 2007, and the Ph.D. degree in electrical engineering from the University of Maryland, College Park, in 2013.

He is currently an Electronics Engineer and a Researcher with U.S. Naval Research Laboratory (NRL), Washington, DC, USA. Since 1994, he has been worked on more than two dozen space missions, often as the Principal Investigator. He was a coordinator and editor for two NRL-led space solar power reports, one authored or coauthored in 2009, and the other in 2019. He has managed large, multidisciplinary teams as the Electrical Segment Lead for several critical space programs, and overseen a portfolio of power beaming and space solar projects. His research interests include power beaming, novel space systems and technologies, renewable energy sources, and efficacy in K-12 Science, Technology, Engineering, and Mathematics (STEM) education. He has authored more than 50 technical publications and holds a U.S. patent, with others pending. He was the author of the space solar chapter in the third edition of Future Energy, and he has made numerous appearances in international television, radio, print, and online media, as a Subject Matter Expert on space solar and power beaming, including as a TEDx Speaker.

Dr. Jaffe has thrice been the recipient of the Alan Berman Research Publication Award. He was the recipient of the Vice Admiral Samuel L. Gravely, Jr., STEM and Diversity Champion of the Year Award for 2012. In 2015, he was named the recipient of the Institute of Environmental Sciences and Technology's Maurice Simpson Technical Editors Award. In 2016, he led a team to win the majority of the awards in the Secretary of Defense-sponsored Defense, Diplomacy, and Development (D3) Innovation Summit Pitch Challenge, those for: Innovation, Presentation, Collaboration, and People's Choice. He was served on the technical committee of the International SpaceWire Conference and was a session organizer for several years of the IEEE Aerospace Conference.

**BRIAN H. SIMAKAUSKAS** received the B.S. degree in electrical engineering from the University of Massachusetts, Amherst, MA, USA, in 2010, and the M.S. degree in electrical engineering from the University of Colorado, Boulder, CO, USA, in 2015.

From 2010 to 2016, he was with ProSensing, Inc. of Amherst, MA, USA, as a Microwave Systems Engineer in the design, integration, and calibration of ground-based cloud radar systems. As a Graduate Researcher with the Antenna Research Group, University of Colorado, his work focused on antenna feed design and fabrication for shipborne applications. Since 2016, he has been with MIT Lincoln Laboratory, as a Technical Staff Member of Space Systems and Technology Division, focusing on radar technology and concepts. He is currently the Deputy Technical Manager with Lincoln Space Surveillance Complex, Westford, MA, USA.

**TREVOR MAYHAN** received the bachelor's degree in mechanical engineering from the University of Massachusetts Amherst, Amherst, MA, USA, in 2018, with a primary focus on aerospace systems and fluid dynamics. His undergraduate research consisted of developing methods for rapid and accurate 3D modeling of small reptiles and amphibians in the laboratory and in the field.

Since 2018, he has been a Mechanical Engineer with Space Systems and Technology Division, MIT Lincoln Laboratory, where he has contributed to multiple upgrades to the Lincoln Space Surveillance Complex. In 2019, he led the implementation of a new encoder and control system in the Millstone Hill Radar, capable of accuracies within ten millidegrees. In addition, he played a critical role in the fabrication and installation of a new low noise W-band cryogenic receiver in the Haystack Ultrawideband Satellite Imagine Radar (HUSIR). His current work is focused on developing a new approach for rotary cable wraps for implementation into large radar systems.